



New evidence for upper Permian crustal growth below Eifel, Germany, from mafic granulite xenoliths

Cliff S. J. Shaw

Department of Earth Sciences, University of New Brunswick, 2 Bailey Drive,
Fredericton, E3B 5A3, New Brunswick, Canada

Correspondence: Cliff S. J. Shaw (cshaw@unb.ca)

Received: 2 October 2020 – Revised: 24 February 2021 – Accepted: 14 March 2021 – Published: 29 April 2021

Abstract. Granulite xenoliths from the Quaternary West Eifel Volcanic Field in Germany record evidence of magmatism in the lower crust at the end of the Permian. The xenoliths sampled two distinct bodies: an older intrusion (ca. 264 Myr old) that contains clinopyroxene with flat, chondrite-normalised rare earth element (REE) profiles and a younger (ca. 253 Myr old) intrusion that crystallised middle-REE-rich clinopyroxene. The younger body is also distinguished based on the negative Sr, Zr and Ti anomalies in primitive mantle-normalised multi-element plots. REE-in-plagioclase–clinopyroxene thermometry records the magmatic temperature of the xenoliths (1100–1300 °C), whereas Mg-in-plagioclase and Zr-in-titanite thermometry preserve an equilibration temperature of ca. 800 °C. These temperatures, together with a model of the mineral assemblages predicted from the composition of one of the xenoliths, define the pressure of crystallisation as ~ 1 GPa. The xenoliths also preserve a long history of reheating events whose age ranges from 220 to 6 Myr. The last of these events presumably led to breakdown of garnet; formation of symplectites of orthopyroxene, plagioclase and hercynite; and redistribution of heavy rare earth elements into clinopyroxene. The data from the West Eifel granulite xenoliths, when combined with the existing data from granulites sampled in the East Eifel, indicate that the lower crust has a long a complex history stretching from at least 1.6 Ga with intrusive events at ca. 410 and 260 Ma and reheating from the Triassic to late Miocene.

1 Introduction

Crustal xenoliths in volcanic rocks carry valuable information about deep subsurface geology and petrology that cannot be accessed in any other way. The textures, mineral assemblages and compositions of the xenoliths provide information on the age of the sampled crust, the pressure and temperature conditions of formation/equilibration. Knowledge of these permits correlation with regional- and continent-scale tectonic events. In particular, xenoliths of granulite facies metamorphic rocks carry information on the petrology and textural evolution of the lower crust (Rudnick and Goldstein, 1990) and may be important in understanding interactions between mantle-derived magmas and the deep lithosphere (Ernst and Liou, 2008).

The nature of the crust and mantle in the Eifel volcanic fields of Germany has been of interest for more than 4 decades because of the young age of volcanism (Schnepf

and Hradetzky, 1994; Nowell et al., 2006; Shaw et al., 2010; Mertz et al., 2015) and the occurrence of P- and S-wave anomalies in the sub-Eifel mantle (Ritter et al., 2001; Keyser et al., 2002). Mantle xenoliths from the West Eifel field have attracted attention because they record multiple metasomatic events that have advanced our understanding of the evolution of the lithospheric mantle and the asthenospheric magmas that have interacted with it (Lloyd and Bailey, 1975; Witt-Eickschen et al., 1998, 2003; Shaw et al., 2005; Mertz et al., 2015; Shaw et al., 2018). Although the lower crust is an important part of the deep lithosphere, its age and evolution in the Eifel region are poorly understood. Up to now, lower-crustal xenoliths have been described from only one location in the East Eifel (Illies et al., 1979; Okrusch et al., 1979; Stosch et al., 1986; Stosch, 1987; Loock et al., 1990; Mengel et al., 1991; Stosch et al., 1992). The East Eifel samples are garnet-bearing mafic granulites and amphibole-

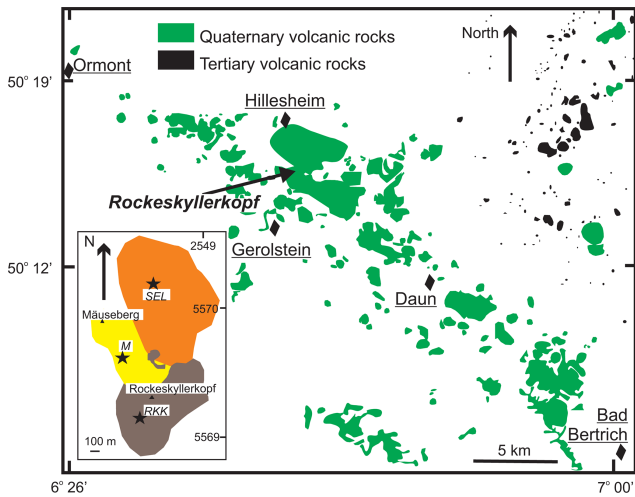


Figure 1. Distribution of Tertiary and Quaternary volcanic rocks in the West Eifel Volcanic Field. Towns are indicated by diamonds. The distribution of the three volcanic centres in the Rockeskyllerkopf Volcanic Complex (RVC) is shown in the inset. These are, from oldest to youngest, the SEL (South East Lammersdorf), M (Mäuseberg) and RKK (Rockeskyllerkopf) centres. Coordinates in the inset map refer to Rheinland Pfalz Topographische Karte Nr 5705 (Gauß–Krüger coordinate system). Regional geology modified from Büchel (1991); geology of the RVC modified from Shaw et al. (2010).

lites that comprise plagioclase, clinopyroxene, garnet, hornblende, orthopyroxene, scapolite, biotite, quartz and titanite.

Seismic studies in the Rhine graben region, of which the Eifel volcanic fields are a part, indicate a minimum depth to the Moho of ca. 25 km (Prodehl, 1981; Prodehl et al., 1992), which suggests a minimum pressure of ca. 0.75 GPa at the Moho. Wörner et al. (1982) used data from seismic surveys, xenoliths and surface geology studies to develop a model of the crust in the East Eifel: this model has 2–5 km of Devonian sedimentary rocks overlying 15–18 km of low-grade metamorphic rocks and a 5 km thick high-grade granulitic lower crust. Seiberlich et al. (2013) showed that the lithosphere–asthenosphere boundary is at 41 ± 5 km below the Eifel and that the Moho is at 27–30 km depth.

This study examines the petrology and age of a new suite of quartz- and garnet-bearing mafic granulites that occur within the well-studied Rockeskyllerkopf Volcanic Complex in the West Eifel Volcanic Field (Shaw and Eyzaguirre, 2000; Shaw, 2009a; Shaw et al., 2010; Shaw and Woodland, 2012; Shaw et al., 2018). The occurrence of accessory titanite in these xenoliths affords the opportunity to obtain robust geochronological information that will help to refine our understanding of the evolution of the crust below the Eifel volcanic fields.

2 Regional and sample site geology

The West Eifel Volcanic Field (Fig. 1) was erupted onto Devonian and Triassic basement. Volcanism began ~ 940 kyr BP, and the last known eruption was ~ 11 kyr BP (Hajdas et al., 1995; Zolitschka et al., 1995; Nowell et al., 2006). The field trends NW–SE and comprises around 240 volcanic centres, including maars, tuff rings, scoria cones and lava flows, with a total erupted volume of ca. 1.7 km^3 (Büchel and Mertes, 1982; Mertes, 1983; Mertes and Schmincke, 1985). The granulite xenoliths for this study were collected from the Rockeskyllerkopf volcanic centre (Fig. 1, inset). This complex comprises three distinct eruptive centres that range in age from 474 ± 39 to 360 ± 60 kyr with evidence for at least one long break in activity in the form of a 1 m thick palaeosol (Mertes and Schmincke, 1983; Shaw et al., 2010). The granulite xenoliths were collected from the same horizons in the South East Lammersdorf (SEL) centre that host the peridotite and clinopyroxenite xenoliths and clinopyroxene and phlogopite megacrysts described by Shaw and Eyzaguirre (2000) and Shaw et al. (2005, 2018). Granulite xenoliths are extremely rare in these deposits. There are only 5 samples from a high-pressure xenolith suite of more than 700 samples.

3 Analytical methods

Major element compositions of clinopyroxene and plagioclase were determined by JEOL 733 electron probe using an accelerating voltage of 15 kV and a beam current of 20 nA. Natural and synthetic clinopyroxene, hornblende, pyrope, albite and anorthite were used for standardisation. Counting times of 40 s were used on peak positions, and background positions were counted for 20 s each on either side of the peak. The resulting data were reduced using a ZAF correction.

Trace element compositions and U–Pb in titanite were measured using a Resonetics S-155-LR excimer laser and an Agilent 7700x quadrupole inductively coupled plasma mass spectrometer, both located at the University of New Brunswick. Ablations were done with a carrier gas of He (300 mL min^{-1}) and Ar (930 mL min^{-1}); for U–Pb analyses sensitivity was increased using a downstream injection of $2 \text{ mL min}^{-1} \text{ N}_2$. Titanite was analysed with a laser energy of 4 J cm^{-2} , a repetition rate of 5 Hz and a $33 \mu\text{m}$ crater diameter. BLR-1 ($1047.1 \pm 0.4 \text{ Ma}$) and MKED ($1521.02 \pm 0.055 \text{ Ma}$) were used as primary and secondary standards respectively (Aleinikoff et al., 2007; Spandler et al., 2016). Zr concentrations were measured using NIST 610 as a standard and the measured Ca content as an internal standard. Common lead corrections were applied using the net ^{204}Pb signal, and the age estimated based on measurements of $^{206}\text{Pb}/^{238}\text{U}$ and the common lead ratio evolution curves presented by Kramers and Tolstikhin (1997). Common lead cor-

rections were applied for $^{204}\text{Pb} > 50$ cps and 1σ internal error of $< 25\%$. Data were processed with Iolite 3.7 (Paton et al., 2011) and the VizualAge data reduction, UcomPbine (Chew et al., 2014). A complete listing of analytical and correction data are given in Supplement S1.

Trace elements in clinopyroxene and plagioclase were analysed using a $60\mu\text{m}$ spot and 0.15 mJ laser energy at 10 Hz with a fluence of 2.1 J cm^{-2} . For elements with multiple naturally occurring isotopes the following were measured: ^{47}Ti , ^{51}V , ^{52}Cr , ^{60}Ni , ^{69}Ga , ^{88}Sr , ^{90}Zr , ^{139}La , ^{140}Ce , ^{146}Nd , ^{147}Sm , ^{151}Eu , ^{161}Dy , ^{167}Er , ^{172}Yb , ^{175}Lu and ^{178}Hf . A gas blank was run before each measurement. Raw data were processed using Iolite 3.5 (Paton et al., 2011) with standard reference values for NIST 612 (Pearce et al., 1997) and the concentrations of ^{29}Si and ^{44}Ca determined by electron probe as internal standards. NIST 610 was measured intermittently to monitor precision and accuracy, which is estimated as $\sim 5\%$. A complete listing of major and trace element analyses of clinopyroxene and plagioclase is provided in the Supplement (S2 and S3). Examination and analysis of symplectites and oxides were done with a JEOL 6400 scanning electron microscope with an EDAX energy dispersive X-ray analysis system. Analyses were made at an accelerating voltage of 15 kV , beam current of 1 nA and count times of 60 s .

4 Petrography and classification

The five granulite xenoliths (Table 1) found in the SEL deposits are rounded to oblate spheroids with a maximum diameter of 5 cm . One sample is massive; four are layered. Three of the xenoliths have fine-grained, symplectitic intergrowths of orthopyroxene, hercynite and calcic plagioclase (Fig. 2a, b). Analyses of 100 by $100\mu\text{m}$ areas of these symplectites and recombination of the phases based on their modal abundance and composition (Table 2) indicate that they have the approximate composition of garnet (almandine: $41\text{--}48$ mole %; andradite/grossular: $16\text{--}22$ mole %; and pyrope: $23\text{--}26$ mole %). The interpretation of the symplectites as the product of garnet is supported by their shape and the similarity in texture with experimentally produced garnet breakdown (Obata et al., 2014). Hereafter, references to garnet in the observed phase assemblage refer to the interpretation of the original nature of the symplectites.

The layers in the xenoliths are 0.5 to 1 cm thick and are defined by variations in the proportion of plagioclase and clinopyroxene in three samples and by the presence of the breakdown products of garnet in the fourth. The grain size of the main phases in the xenoliths is $1\text{--}2\text{ mm}$.

All five samples are mafic granulites. Three (10E, 13E and 13H) consist of garnet, plagioclase and clinopyroxene with lesser quartz and scapolite. Garnet breakdown products occur in fine-grained black layers, and accessory titanite is common. The two garnet-free samples are dominated

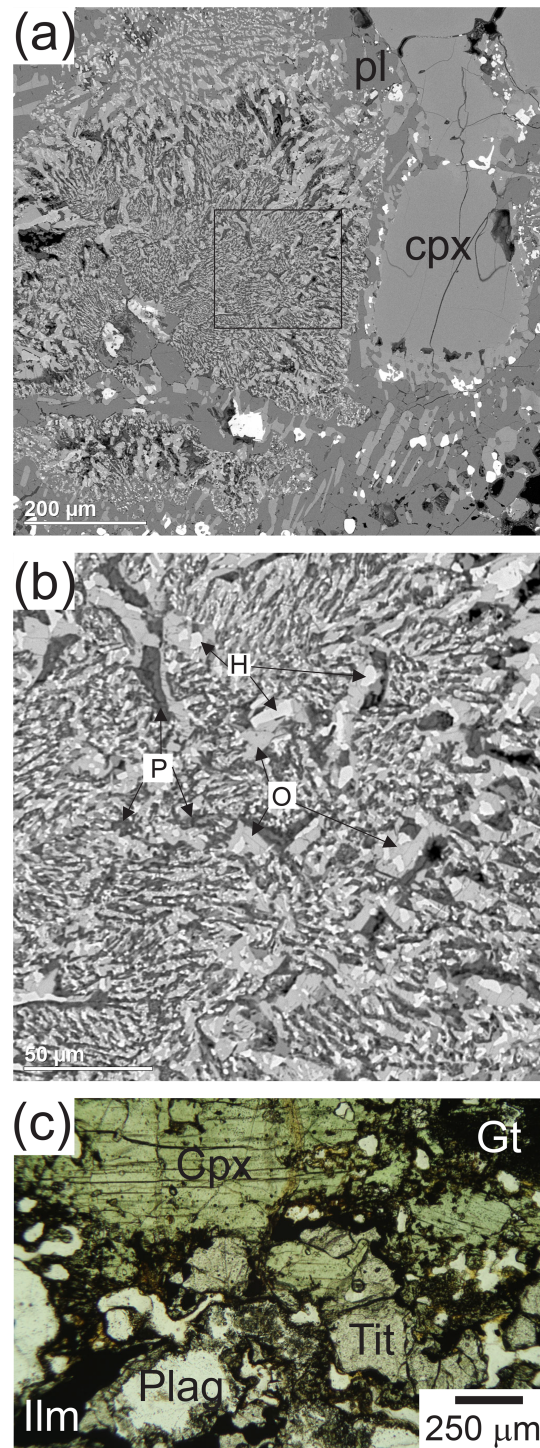


Figure 2. (a) Backscattered electron image of sample 13H showing a pseudomorph after garnet surrounded by calcic plagioclase. Right side of the image shows a coarse clinopyroxene decorated with neoblasts of clinopyroxene. The region in the pseudomorph outlined by the square is shown in more detail in panel (b). (b) Inter-growth of hercynite (H), orthopyroxene (O) and plagioclase (P) in garnet pseudomorph. (c) Photomicrograph of sample 10E showing titanite (Tit) intergrown with plagioclase (Plag), ilmenite (Ilm) and clinopyroxene (Cpx). Garnet breakdown products are visible in the top right of the image.

Table 1. Sample description and summary of age data.

Sample	Texture and mineralogy	Clinopyroxene composition	Age (Myr)
Type 1 clinopyroxene			
11L	1–2 cm thick layers. Plagioclase, clinopyroxene, oxides, titanite, trace quartz and trace altered biotite.	Chondrite-normalised REE abundances between 1 and 10 times chondrite. Patterns are flat. Primitive mantle-normalised multi-element plots show a positive Hf anomaly.	259.4 ± 4.7
13E	1 cm layers, garnet breakdown products present in one layer near the edge of the xenolith. Plagioclase, clinopyroxene, scapolite, oxides, quartz and titanite.		266.2 ± 1.4
Type 2 clinopyroxene			
10E	1–2 cm thick layers defined by garnet breakdown products. Clinopyroxene, plagioclase, quartz, titanite and scapolite.	Chondrite-normalised REE patterns show enrichment in Pr to Dy. HREE abundances are variable, ranging from sub-chondritic to ~20 times chondrite.	253.7 ± 2.5
13H	Massive. Clinopyroxene, plagioclase, oxides, quartz and garnet breakdown products.	Primitive mantle-normalised multi-element plots show negative Sr, Zr and Ti anomalies.	
10L	Diffuse layering ~0.5 mm thick. Plagioclase, clinopyroxene, oxides, quartz and trace titanite.		

Table 2. Phases in symplectite in sample 13H – energy dispersion spectroscopy (EDS) analyses.

wt %	Hercy	Hercy	Opx	Opx	Opx	Opx	An	An	An	Area scan	Area scan	Mode
SiO ₂	0.36	1.54	45.66	48.93	50.38	50.56	45.10	44.39	47.70	38.50	41.32	38.23
TiO ₂	0.12	0.85	0.00	0.06	0.32	0.24	0.06	0.00	0.00	0.34	0.45	0.16
Al ₂ O ₃	47.88	39.05	7.16	3.77	4.52	4.87	35.61	34.99	32.91	24.69	26.29	26.43
FeO	42.97	49.33	33.15	28.60	20.83	19.79	1.51	1.99	1.22	21.54	15.74	18.16
MnO	0.79	0.58	1.37	1.32	0.84	0.68	0.09	0.17	0.14	0.85	0.40	0.55
MgO	7.44	8.00	9.80	15.28	20.81	21.09	0.29	0.36	0.30	6.89	5.13	7.23
CaO	0.09	2.48	2.56	1.70	1.88	2.48	16.44	16.88	15.30	6.37	9.30	8.45
Na ₂ O	0.22	0.24	0.00	0.11	0.13	0.07	0.81	0.89	2.35	0.58	0.89	0.71
K ₂ O	0.04	0.09	0.07	0.03	0.09	0.07	0.06	0.15	0.08	0.26	0.21	0.08
Total	99.92	99.92	99.76	99.80	99.81	99.83	100.01	99.81	99.99	100.01	99.74	99.99

Hercy: hercynite. Opx: orthopyroxene. An: plagioclase. Area scan: scan of a 100 × 100 μm region at the centre of two different symplectite regions. Mode: composition based on recombination of the average composition of each mineral phase in the proportions 19.2 % hercynite, 33.4 % orthopyroxene and 47.5 % anorthite (determined from image analysis of Fig. 2c).

by clinopyroxene and plagioclase with lesser quartz and titanite. One sample has traces of altered biotite. Plagioclase in all the samples shows evidence of deformation: lenticular, kinked and offset twin lamellae (Vernon, 2004). Where present, quartz shows well-developed undulose extinction. Both plagioclase and quartz contain numerous fluid inclusions. Scapolite partly to completely replaces plagioclase in samples 10E and 13H. Clinopyroxene is green, anhedral, strongly pleochroic and unzoned, though the cores of most grains are rich in fluid and opaque inclusions. The Fe–Ti oxides are two phase, with a hercynite and ulvöspinel phase. Titanite forms 0.2–0.8 mm anhedral grains interstitial to plagioclase, clinopyroxene and Fe–Ti oxides (Fig. 2c).

5 Mineral compositions

5.1 Clinopyroxene

Clinopyroxene in the xenoliths is aluminian diopside (Table 3), though each sample defines a distinct cluster of compositions in terms of xMg [molar Mg/(Mg + Fe^{tot}) · 100]. Clinopyroxene in garnet-free granulites shows rim–core zonation; rims are typically slightly more magnesian and less sodic than cores. Overall, clinopyroxene shows increasing TiO₂, Al₂O₃ and to a lesser extent Na₂O with decreasing xMg (Fig. 3a–c). Clinopyroxene in the garnet-bearing samples overlaps in composition with that in the garnet-free samples but extends to higher xMg (Fig. 3).

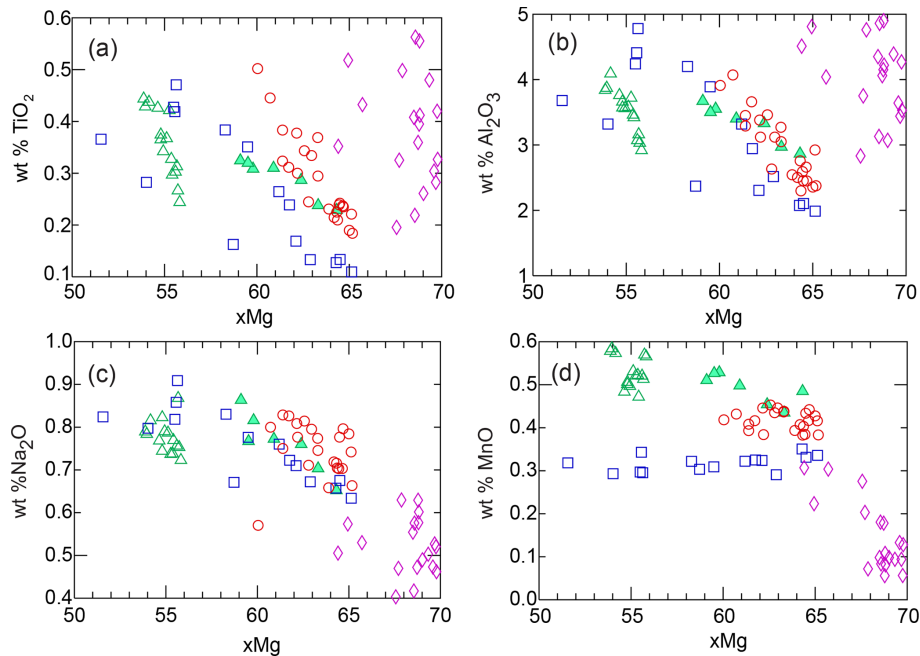


Figure 3. Major element composition of clinopyroxene. (a) xMg vs. weight percent TiO_2 . (b) xMg vs. weight percent Al_2O_3 . (c) xMg vs. weight percent Na_2O . (d) xMg vs. weight percent MnO.

The same trends of increasing TiO_2 , Al_2O_3 and Na_2O with decreasing xMg are seen in these samples; however, the clinopyroxene in garnet-bearing samples is depleted in MnO (Fig. 3a–d).

On the basis of the trace element composition of clinopyroxene the samples can be subdivided into two groups (Table 3, Fig. 4). Type 1 has one garnet-free and one garnet-bearing sample (11L and 13E respectively). Clinopyroxene in these samples shows nearly flat chondrite-normalised REE profiles and a distinct positive Hf anomaly on a primitive mantle-normalised multi-element plot. The garnet-free sample has low Co (< 20 ppm) and high Sc (40–80 ppm) and Cr (100–200 ppm) compared to the garnet-bearing sample. Type 2 clinopyroxene also occurs in garnet-free (10L) and garnet-bearing samples (10E and 13H). In these samples, clinopyroxene has convex upward chondrite-normalised REE patterns with moderate light-REE (LREE) depletion compared to middle REE (MREE). Clinopyroxene in the garnet-free samples has 20–30 times chondrite heavy REE (HREE). The two garnet-bearing samples have clinopyroxene with a much wider range of HREE content, from strongly depleted with convex upward to flat REE patterns similar to those of the garnet-free sample. Type 2 clinopyroxene is also distinct from type 1 clinopyroxene in the negative Sr, Zr and Ti anomalies on the primitive mantle-normalised multi-element plot.

Several samples show small variations in trace element composition across the clinopyroxene crystals (Fig. 5). There is minor zonation in Ti and Zr, with cores slightly enriched

relative to rims. In the garnet-bearing samples, Yb and the other heavy rare earth elements are enriched at the edge of the crystals, where they are in contact with the garnet breakdown products (Fig. 5a, c). In contrast, clinopyroxene rims in the garnet-free sample are HREE depleted.

5.2 Plagioclase

Garnet-free granulites 10L and 11L have average plagioclase compositions of An_{45} and An_{42} respectively, and the garnet-bearing sample (10E) has plagioclase of An_{46} (Fig. 6a). In contrast, the other two garnet-bearing samples have much more calcic plagioclase (13E: An_{66} ; 13H: An_{80} ; Table 4). The anorthite content of plagioclase has a positive correlation with the xMg of clinopyroxene.

In the symplectites, the plagioclase is An_{90} . Unlike the coarser plagioclase in the layers, the plagioclase in the symplectites contains up to 2 wt % FeO (Table 2).

The three samples for which trace elements were determined show a variable positive Eu anomaly, small in 11L and large in 13H with 10L intermediate (Fig. 6b). Sample 11L is distinct in its Sr enrichment (Table 4), which correlates with the Sr-rich composition of coexisting clinopyroxene.

5.3 Oxides

The abundant oxide grains in sample 13H have cores of ilmenite mantled by ulvöspinel (Table 5). In the symplectites, the oxide is hercynite (Table 2).

Table 3. Major and trace element of clinopyroxene.

Sample type	11L 1	11L 1	13E 1	13E 1	10E 2	10E 2	13H 2	13H 2	10L 2	10L 2
wt %										
SiO ₂	49.27	49.64	50.16	49.78	49.91	49.71	49.71	49.90	51.14	50.83
TiO ₂	0.44	0.36	0.43	0.37	0.22	0.21	0.33	0.52	0.23	0.32
Al ₂ O ₃	3.84	3.66	4.24	3.68	2.92	2.30	3.75	4.81	2.86	3.50
Cr ₂ O ₃	0.03	0.03	0.01	0.03	0.03	0.04	0.01	0.02	0.02	0.01
FeO	13.94	13.80	13.56	15.31	11.13	11.15	10.73	11.46	11.43	12.46
MnO	0.58	0.50	0.30	0.32	0.42	0.40	0.20	0.22	0.48	0.53
MgO	9.13	9.38	9.48	9.14	11.65	11.29	12.61	11.90	11.55	10.27
CaO	21.78	22.28	22.27	21.32	21.62	22.88	21.38	20.65	21.90	22.24
Na ₂ O	0.79	0.74	0.82	0.82	0.74	0.70	0.47	0.57	0.65	0.77
Total	99.80	100.4	101.26	100.76	98.64	98.68	99.19	98.06	100.27	100.92
ppm										
Sc	51.4	52.8	27.3	65.3	37.9	45.6	90.7	79.7	77.2	49.6
Ti	1642	1641	2033	2117	1103	1091	1638	2229	1878	1251
V	213	214	321	303	235	210	284	416	373	285
Cr	145	125	21	78	48	18	181	197	51	26
Co	14.4	12.8	57.8	71.5	35.8	31.9	77.8	78.2	63.4	44.4
Ni	9.7	6.3	79.9	70.7	46.8	44.1	147.2	143.3	84.7	57.3
Rb	0.03	bdl	0.24	bdl	0.19	bdl	0.45	0.10	0.02	0.01
Sr	42.6	35.1	46.9	52.1	9.8	11.3	11.2	15.0	24.2	13.2
Y	2.3	2.8	4.3	4.0	14.0	5.1	18.8	12.5	57.7	34.5
Zr	35.2	39.4	56.3	45.8	25.2	16.0	20.1	40.0	47.7	25.6
Nb	0.01	bdl	0.19	bdl	0.27	0.01	0.35	0.17	0.10	0.03
La	1.28	0.54	0.56	0.66	0.62	0.99	2.26	1.74	0.74	0.69
Ce	2.95	1.83	2.40	1.86	1.39	3.32	8.98	6.15	8.26	2.51
Pr	0.39	0.32	0.43	0.32	0.34	0.50	1.66	1.30	2.73	0.76
Nd	1.91	2.13	2.29	1.43	3.40	2.56	9.58	10.82	21.17	7.59
Sm	0.46	0.56	0.56	0.61	1.83	0.72	3.77	4.72	8.83	4.69
Eu	0.10	0.12	0.16	0.14	0.48	0.27	1.41	1.56	2.25	1.30
Gd	0.38	0.66	0.72	0.72	2.84	1.08	4.54	5.68	11.54	6.50
Tb	0.08	0.09	0.12	0.11	0.49	0.24	0.76	0.70	1.94	1.18
Dy	0.41	0.61	0.76	0.53	3.11	1.13	4.32	3.45	12.14	7.40
Ho	0.08	0.10	0.18	0.13	0.61	0.20	0.71	0.53	2.50	1.49
Er	0.22	0.33	0.43	0.43	1.27	0.41	1.76	0.86	6.04	3.72
Tm	0.03	0.03	0.06	0.06	0.17	0.05	0.24	0.13	0.74	0.50
Yb	0.38	0.28	0.50	0.47	1.12	0.41	1.42	0.59	5.49	3.22
Lu	0.07	0.07	0.12	0.12	0.18	0.07	0.22	0.06	0.78	0.53
Hf	1.65	1.78	2.17	2.45	1.83	1.47	1.72	2.84	3.16	1.75

bdl: below detection limits.

6 Geothermometry

The temperature of equilibration of the xenoliths has been calculated using three independent methods: the Mg-in-plagioclase thermometer of Faak et al. (2013), for samples with plagioclase more calcic than An₅₀; the REE-in-plagioclase–clinopyroxene thermometer of Sun and Liang (2017); and the Zr-in-titanite thermometer (Hayden et al., 2008). The results are summarised in Table 6. The temperature calculated using the Mg-in-plagioclase thermometer is significantly lower than that calculated using the REE-in-

plagioclase–clinopyroxene thermometer. The faster diffusion of Mg compared to REE in plagioclase (Faak et al., 2013; Sun and Liang, 2017) gives a higher closure temperature for the REE-in-plagioclase–clinopyroxene geothermometer, which may record the original crystallisation temperature. Conversely, because of its lower closure temperature, Mg in plagioclase is more likely to record a metamorphic equilibration temperature. The temperature determined from REE in plagioclase ranges from 1090 to 1330 °C, i.e. a magmatic temperature range, whereas Mg in plagioclase gives tempera-

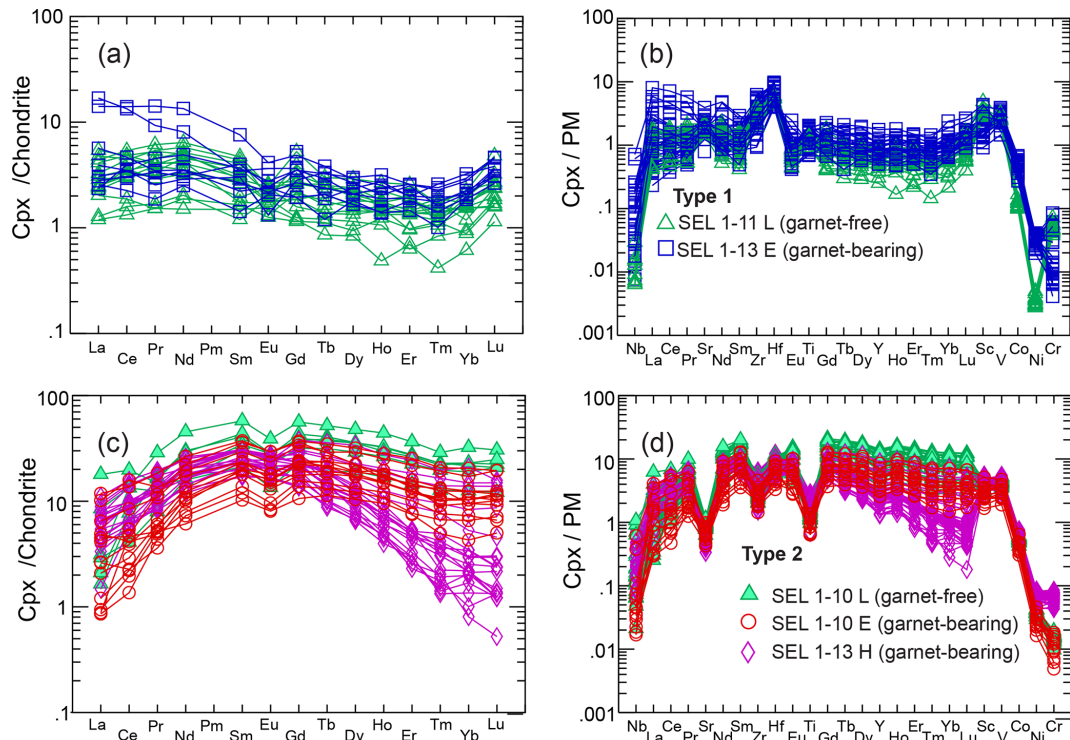


Figure 4. Chondrite-normalised rare earth element and primitive mantle normalised incompatible element patterns for clinopyroxene. Normalisation factors from Sun and McDonough (1989). **(a)** Chondrite-normalised rare earth element plot of type 1 clinopyroxene. **(b)** Primitive mantle-normalised multi-element plot type 1 clinopyroxene. **(c)** Chondrite-normalised rare earth element plot type 2 clinopyroxene. **(d)** Primitive mantle-normalised multi-element plot of type 2 clinopyroxene.

ture in the range 680 to 930 °C, which is closer to the temperature expected for equilibration of lower-crustal granulites in this region (Loock et al., 1990).

Zirconium contents in the titanites are extremely variable. In sample 13E, Zr contents range between 163 and 1483 ppm with an average of 968 ppm. Samples 11L and 10E have smaller ranges and average Zr contents of 641 and 517 ppm respectively. Application of the Zr-in-titanite thermometer gives temperatures ranging from 783 to 818 °C. These temperatures were calculated for titanite in quartz-bearing samples assuming both aSiO₂ and aTiO₂ set to unity. Slightly lower activities will give temperatures that are lower by 10–20 °C. Samples 11L and 13H have a unimodal temperature distribution with maxima at 800–810 and 820–830 °C respectively. Sample 10E gives a bimodal temperature distribution with maxima at 780 and 810 °C. The Zr-in-titanite temperature range overlaps with those of Mg in plagioclase, indicating that both record lower-crustal equilibration temperature for the xenoliths.

7 Geochronology

U–Pb data for titanite in three samples (Fig. 7, Supplement S1) define a broad array in Tera–Wasserburg plots. The

upper intercept ages of the three samples do not overlap, but all are upper Permian (253–266 Myr). The lower intercept ages range from Triassic to late Miocene (Fig. 7).

The lack of overlap (within the error bounds of the age determinations) suggests that the xenoliths represent samples from at least two distinct sources: one with an age of ~264 Myr (11L and 13E) and a second of ~253 Myr (10E), in agreement with different REE signatures of clinopyroxene. Frost et al. (2001) and Hartnady et al. (2019) proposed that the closure temperature of titanite is above 660 and possibly above 800 °C. The temperatures determined from the Zr-in-titanite and Mg-in-plagioclase thermometers suggest that the titanites may have been close to or above their closure temperature. This is in accord with the wide spread of the data on Tera–Wasserburg plots, suggesting that there has been significant resetting of the U–Pb systematics due to lead loss during reheating events. The probability density plot (Fig. 7d) suggests a major disturbance at 230–200 Ma with almost continuous disturbance occurring to ~6 Ma with a gap between 20 and 30 Ma. Even though there is some possible reheating, Hartnady et al. (2019) suggested that the extremely low diffusivity of Pb implies that titanite can be used to reliably date its crystallisation. This is discussed in more detail below.

Table 4. Major and trace element composition of plagioclase.

Sample	11L	11L	13E	10E	10E	13H	13H	10L	10L
wt %									
SiO ₂	57.49	57.05	53.13	55.97	56.10	46.35	47.90	57.22	55.87
Al ₂ O ₃	25.91	26.55	28.25	28.08	27.26	34.55	32.93	26.98	26.22
FeO	0.10	0.37	0.59	0.09	0.18	0.39	0.32	0.12	0.38
MnO	0.00	0.01	bdl	0.01	0.04	0.01	bdl	bdl	bdl
CaO	8.53	9.15	11.92	9.69	9.88	17.49	15.59	8.95	9.63
Na ₂ O	6.76	6.35	4.58	6.14	5.73	1.67	2.66	6.29	5.97
K ₂ O	0.42	0.59	0.48	0.41	0.55	0.04	0.03	0.36	0.34
total	99.22	100.07	98.96	100.39	99.75	100.50	99.42	99.92	98.40
ppm									
Ti	197	285	na	na	na	14	18	29	11
Sr	1854	1977	na	na	na	357	548	800	747
Y	0.53	0.76	na	na	na	0.84	0.39	0.07	0.18
La	2.15	2.96	na	na	na	2.82	2.42	2.47	1.98
Ce	1.75	2.14	na	na	na	5.81	3.81	3.64	3.17
Pr	0.20	0.22	na	na	na	0.48	0.31	0.32	0.24
Nd	0.84	1.08	na	na	na	1.73	1.09	1.15	0.80
Sm	0.04	0.14	na	na	na	0.22	0.15	bdl	bdl
Eu	0.04	0.12	na	na	na	0.56	0.54	0.14	0.28
Gd	0.11	bdl	na	na	na	0.11	bdl	bdl	bdl
Tb	bdl	0.01	na	na	na	0.03	bdl	bdl	bdl
Dy	0.07	0.14	na	na	na	bdl	bdl	bdl	bdl
Ho	0.02	0.02	na	na	na	0.02	bdl	bdl	0.01
Er	0.03	0.08	na	na	na	0.04	bdl	bdl	bdl
Tm	bdl	bdl	na	na	na	bdl	bdl	bdl	bdl
Yb	0.08	bdl	na	na	na	bdl	bdl	bdl	bdl
Lu	bdl	0.03	na	na	na	bdl	bdl	bdl	bdl

bdl: below detection limits; na: not analysed.

Table 5. Ilmenite and Ulvöspinel analysis (EDS) from sample 1–13H.

wt %	Ilm	Ulvsp	Ilm	Ulvsp	Ilm	Ulvsp	Ilm	Ulvsp
SiO ₂	0.19	0.23	0.22	0.11	0.19	0.18	0.18	0.25
TiO ₂	42.39	22.00	43.66	22.51	41.21	12.83	41.81	19.11
Al ₂ O ₃	0.96	3.04	0.82	3.06	0.91	6.42	0.98	4.85
FeO	52.97	70.98	51.45	69.91	54.27	76.74	53.58	71.29
MnO	0.67	0.81	0.50	0.77	0.50	0.66	0.56	0.60
MgO	2.54	2.69	3.01	3.31	2.57	2.81	2.63	3.41
CaO	0.09	0.04	0.21	0.18	0.17	0.13	0.09	0.24
Na ₂ O	0.07	0.00	0.00	0.00	0.00	0.00	0.00	0.00
Total	99.88	99.78	99.86	99.85	99.82	99.78	99.83	99.75

Ilm: ilmenite; Ulvsp: ulvöspinel.

8 Discussion

8.1 Nature of the protolith

The high temperature recorded by REE-in-plagioclase–clinopyroxene thermometry suggests that these xenoliths preserve at least part of an original igneous mineralogy,

whereas the lower temperature from Mg-in-plagioclase and Zr-in-titanite thermometry may record the equilibration temperature at the base of the crust. The orthopyroxene–plagioclase–hercynite symplectites attest to the breakdown of pre-existing garnet. This leads to the question of whether these xenoliths should be considered truly metamorphic or whether they are lower-crustal cumulates that crystallised ig-

Table 6. Summary of mineral thermometry results (in °C).

Sample	Method			
	REE in plagioclase	Mg exchange		Zr in titanite
		aSiO ₂ = 1	aSiO ₂ = 0.64	
	Sun and Liang (2017)	Faak et al. (2013)	Hayden et al. (2008)	
11L	1268 ± 47	856 ± 39	927 ± 44	799 ± 9
10E	n.d.	n.d.	n.d.	783 ± 25
13H	1331 ± 71	725 ± 28	788 ± 31	818 ± 24
10L	1089 ± 71	632 ± 114	679 ± 126	n.d.

n.d.: not determined.

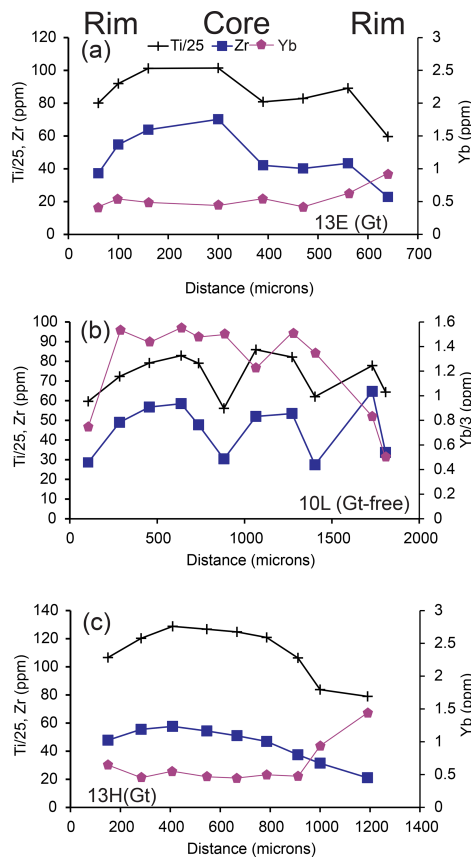
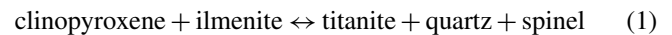


Figure 5. Core-to-rim trace element variation in clinopyroxene. **(a)** Type 1 clinopyroxene (sample 13E) from rim to rim; core is at ~300 μm. Ti and Zr are depleted in the rims. Yb is enriched in the right rim, where the clinopyroxene is in contact with plagioclase and garnet-breakdown products. **(b)** Garnet-free type 2 clinopyroxene (sample 10L) from rim to rim; core is at ~1000 μm. Ti and Zr are depleted in the rims. Yb is depleted in both rims. **(c)** Garnet-bearing type 2 clinopyroxene (Sample 13H) from rim to rim; core is at ~600 μm. Ti and Zr are depleted in the rims. Yb is enriched in the right rim, where the clinopyroxene is in contact with breakdown products of garnet.

neous garnet (cf. Faryad et al., 2018). The variable chondrite-normalised REE patterns and primitive mantle-normalised Sr, Hf and Ti anomalies in clinopyroxene suggest that the samples were derived from at least two different parent magmas.

8.2 Crystallisation conditions and the significance of the titanite ages

Experimental studies of mafic magmas show that assemblages of clinopyroxene, garnet and plagioclase can be produced by high-pressure crystallisation (e.g. Green and Ringwood, 1967). Titanite in mafic rocks can form by a variety of subsolidus reactions (Xirouchakis et al., 2001a, b). In the samples described here, titanite coexists with plagioclase, quartz, clinopyroxene and ilmenite (and ulvöspinel in 13H). The titanite likely formed by a reaction similar to (Xirouchakis et al., 2001a)



as part of subsolidus equilibration. This subsolidus event is likely simply the continuation of cooling after the formation of cumulates. Hirschmann et al. (1997) have shown that subsolidus reactions in the Skaergaard intrusion resulted in formation of titanite by reaction at 690–720 °C, ~0.2 Myr after initial intrusion.

In the present case, the reaction conditions needed for titanite formation by subsolidus reaction can be estimated using the Theriak-Domino thermodynamic calculation program (de Capitani and Brown, 1987; de Capitani and Petrakakis, 2010) and the composition of a xenolith, determined from the mode and mineral compositions. A pseudo-section produced using the thermodynamic database of Berman et al. (1985) indicates that titanite forms at ~1 GPa under the temperature conditions indicated from thermometry (Fig. 8) and that the main mineral assemblage matches that observed. Using this estimated pressure, the magma that formed the parent body of the xenoliths was intruded at a depth of ~30 km. At this depth, a 1 km thick sill emplaced at 1250 °C with the lower contact at 30 km and a 25 °C km⁻¹

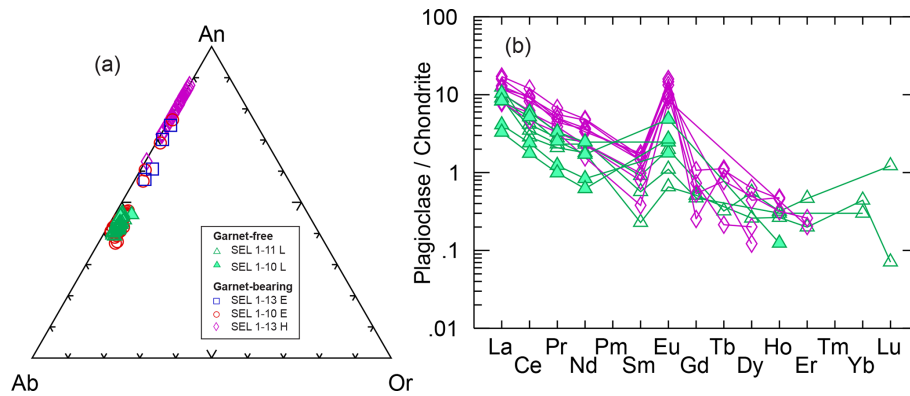


Figure 6. Major and trace element variation in plagioclase. (a) Plagioclase compositions showing that the samples 13E and 13H are significantly more calcic than the two garnet-free samples and sample 10E. (b) Chondrite-normalised REE plot (normalisation values of Sun and McDonough, 1989).

geothermal gradient, mantle density of 3300 kg m^{-3} , crust density of 2900 kg m^{-3} , thermal conductivity of 4.2 and $3.0 \text{ W m}^{-1} \text{ K}^{-1}$ for mantle and crust respectively, and a heat capacity of $1200 \text{ J kg}^{-1} \text{ K}^{-1}$ (Petford and Gallagher, 2001) would equilibrate with the geotherm after 1 to 1.2 Myr, based on the HEAT3D model of Wohletz et al. (1999). Thus, although the U–Pb ages determined for the titanites do not correspond to the primary igneous event, they do closely correspond to the age of the intrusive event(s) that formed the granulites.

8.3 Formation of symplectites

Mineral breakdown reactions may be due to heating prior to xenolith entrainment or to post-entrainment reactions between the xenolith minerals and host (Shaw and Edgar, 1997; Canil and Fedortchouk, 1999; Shaw, 1999; Shaw and Klügel, 2002; Shaw et al., 2006; Shaw, 2009b). Orthopyroxene–plagioclase symplectites are common around garnets in granulite terranes (Harley, 1989) and are interpreted as being related to decompression during exhumation. However, a similar reaction should occur in the case of isobaric heating since in both cases the garnet stability curve is overstepped. In many granulite terranes and where garnet is preserved as megacrysts in kimberlite (Canil and Fedortchouk, 1999; O’Brien and Rötzler, 2003; Tam et al., 2012) it is partly preserved with coronas of variable width of intergrown orthopyroxene and plagioclase, indicating that the reaction period was short enough to leave behind relict garnet. In the samples described here, there is no garnet remaining in any of the samples.

Obata et al. (2014) produced a very similar symplectitic orthopyroxene–plagioclase–spinel assemblage during experimental breakdown of garnet at 0.85 GPa and 1100 °C . The minimum temperature for breakdown in the Rockeskyllerkopf samples is estimated as 925 °C at 1.1 GPa from the phase relations shown in Fig. 8. The rate of symplectite

formation calculated by Dégi et al. (2010) suggests that garnets with a radius of 1 mm could be completely replaced in as little as $40\,000$ years at high temperature ($\sim 1050 \text{ °C}$) and as long as 3 million years near the garnet stability curve.

In sample 13H, clinopyroxene shows a wide range in HREE. Low HREEs are expected for clinopyroxene crystallising in equilibrium with garnet, which would sequester more HREEs than clinopyroxene. High REE or unfractionated REE would result from crystallisation in the absence of garnet. The zonation in the outer part of the clinopyroxene crystals (Fig. 5) can be interpreted as being due to diffusive addition of HREE released by the garnet breakdown. The width of these zones is around $50 \mu\text{m}$. Based on extrapolation of Van Orman et al. (2001) tracer diffusion data for Yb to 925 °C , which is the minimum temperature for garnet breakdown based on phase relations (Fig. 8), these would take ~ 1.5 Myr to form. With heating to 1050 °C , the observed profiles could form in as little as $60\,000$ years. The estimate of the duration of the breakdown event from the kinetics of symplectite formation and diffusion rates are in general agreement. It is not possible to determine the conditions or age of breakdown from the available data. A thermal disturbance large enough to drive breakdown would decay over time, and it is likely that garnet would reform from the symplectite assemblage. For this reason, it seems most likely that the disturbance is young, possibly associated with Tertiary or even Quaternary magmatism. There is evidence of magma accumulations in the lithospheric mantle on this timescale (Shaw et al., 2018). Hence, it is not unreasonable to suggest that magma flux and the increase in temperature that would be associated with it might lead to heating that would affect the granulitic base of the crust and cause garnet breakdown.

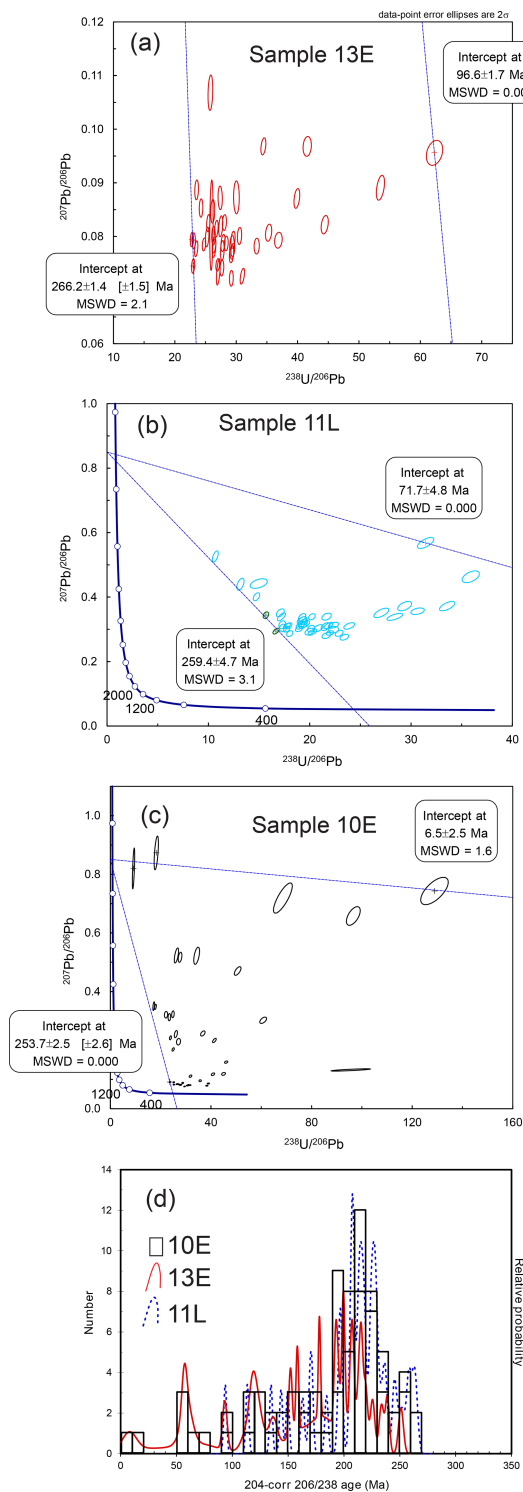


Figure 7. Titanite geochronology. (a–c) Tera–Wasserburg plots for samples 13E, 11L and 10E. Error ellipses are plotted at 2σ . The lines fit to the data give the interpreted crystallisation age (left most intercept), and the minimum disturbed age is given by the lower intercept. (d) Probability density plot for samples 13E, 11L and 10E showing the range of interpreted crystallisation ages and the timing of the interpreted reheating events.

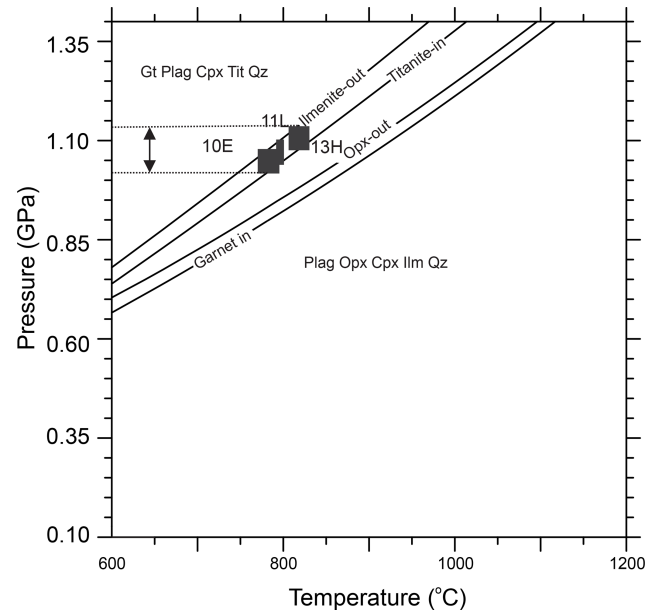


Figure 8. Pseudosection for sample 11L calculated with Theriak-Domino (de Capitani and Brown 1987; de Capitani and Petrakakis, 2010) using the database of Berman et al. (1985). The grey boxes show the estimated temperature for samples 10L, 10E and 13H. Pressure is bracketed by the titanite in- and ilmenite out-curves since both phases are present. This indicates a pressure of 1 to 1.15 GPa for the titanite-forming reaction. Gt: garnet. Plag: plagioclase. Opx: orthopyroxene. Cpx: clinopyroxene. Ilm: ilmenite. Qz: quartz. Tit: titanite. The bulk composition input into the file THERIN is Si (50.491), Ti (1.0306), Al (14.681), Fe (6.409), Mn (0.232), Mg (6.052), Ca (14.497), Na (6.114), K (0.217) and O (?). This composition also gives trace tephroite as a phase at all pressures – this has been omitted from the phase assemblage for simplicity.

9 Geodynamic implications

The only other samples of lower-crustal material from the Eifel region are the granulite xenoliths from Engeln in the East Eifel (Okrusch et al., 1979; Stosch et al., 1986, 1992; Schmincke, 2007). The Engeln samples comprise two suites – one with a depleted mantle model age of ca. 1.6 Gyr with metasomatism at 172 ± 5 Myr and a second suite with an igneous age of 412 ± 81 Myr and reheating events at 170 and 100 Myr.

The late Permian age and interpreted igneous protolith of the granulites from West Eifel suggest growth of the lower crust by addition of mafic magma following the collapse of the Permo-Carboniferous Hercynian Orogen. There is evidence of late Hercynian magmatism across much of north-west Europe from Scotland and the Massif Central (Upton et al., 2004; Berger et al., 2007) to the Southern Permian Basin (Benek et al., 1996; Timmerman et al., 2009) and the Saar-Nahe region of Germany (Schmidberger and Hegner, 1999). In the Eifel region, Meyer (1994) reports porphyry breccia

and tuff in the Permian Wittlich Basin, which lies just south of the West Eifel Volcanic Field. Further west in the Massif Central (France), Féménias et al. (2003) and Berger et al. (2007) reported lower-crustal granulites of similar age (257 ± 6 Myr), which they interpret as fragments of a deep crustal layered intrusion.

The range of lower intercept ages for titanite indicates multiple post-crystallisation reheating events (Fig. 7). The oldest of these events was bracketed between 200–230 Ma and can be speculatively correlated with magmatism associated with the breakup of Pangea (Dèzes et al., 2004; Ziegler and Dèzes, 2005). Marzoli et al. (2014) and Pozsgai et al. (2017) reported Upper Triassic igneous rocks in NW France and in the Pannonian Basin, which they relate to the development of the Central Atlantic Magmatic Province. Large-scale transport of magma into and through the crust at this time could explain the first event of post-equilibration reheating.

Following the peak of reheating recorded at ~ 220 Ma, there was almost continuous disturbance of the U–Pb systematics in titanite until ~ 50 Ma. This is in accord with the conclusions of Ziegler and Dèzes (2005), who suggested that there was thermal re-equilibration of the lithospheric–asthenospheric mantle associated with subsidence of sag basins throughout the Mesozoic. The youngest discordant, Pb-corrected ages of the titanite range from ~ 20 to 6 Myr, which may correlate with formation of a thermal anomaly above what was to become the Eifel plume (Dèzes et al., 2004). The widespread Tertiary volcanic rocks in the neighbouring Hocheifel region range in age from 44 to 35 Myr (Fekiacova et al., 2007), which could also explain some of the reheating.

Together the two suites of granulites from Eifel point to a long history of crustal growth beginning at 1.6 Ga with clearly defined intrusive events at ~ 400 and ~ 260 Ma with numerous periods of metasomatism and reheating.

Data availability. All data are included in the Supplement.

Supplement. The supplement related to this article is available online at: <https://doi.org/10.5194/ejm-33-233-2021-supplement>.

Competing interests. The author declares that there is no conflict of interest.

Acknowledgements. Thanks to Calvin Nash and Stephen Delahunty for producing the thin sections used in this study. Thanks also to Douglas Hall, Stephen Cogswell and Brandon Boucher for their assistance with mineral analysis; Chris Zelt for discussions on the interpretation of the titanite geochronology data; and Johana Gomez for comments on an earlier draft of the manuscript. I am very grateful for the constructive reviews provided by Luca Ziberna and an

anonymous referee and to Riccardo Tribuzio and Elisabetta Rampono for their editorial work. This project was funded through a Discovery Grant from the Natural Sciences and Engineering Research Council of Canada and the Boylen Fund administered by the University of New Brunswick.

Financial support. This research has been supported by the Natural Sciences and Engineering Research Council of Canada (Discovery Grant).

Review statement. This paper was edited by Riccardo Tribuzio and reviewed by Luca Ziberna and one anonymous referee.

References

- Aleinkoff, J. N., Wintsch, R. P., Tollo, R. P., Unruh, D. M., Fanning, C. M., and Schmitz, M. D.: Ages and origins of rocks of the Killingworth dome, south-central Connecticut: Implications for the tectonic evolution of southern New England, *Amer. J. Sci.*, 307, 63–118, 2007.
- Benek, R., Kramer, W., McCann, T., Scheck, M., Negendank, J. F. W., Korich, D., Huebscher, H. D., and Bayer, U.: Permo-Carboniferous magmatism of the Northeast German Basin, *Tectonophysics*, 266, 379–404, 1996.
- Berger, J., Féménias, O., Coussaert, N., Mercier, J.-C. C., and Demaiffe, D.: Cumulating processes at the crust-mantle transition zone inferred from Permian mafic-ultramafic xenoliths (Puy Beaunit, France), *Contrib. Mineral. Petrol.*, 153, 557–575, 2007.
- Berman, R. G., Brown, T. H., and Greenwood, H. J.: An internally consistent thermodynamic database for minerals in the system Na₂O–K₂O–CaO–MgO–FeO–Fe₂O₃–Al₂O₃–SiO₂–TiO₂–H₂O–CO₂, Atomic Energy of Canada, Technical Report 377, Pinawa, Manitoba, 1985.
- Büchel, G.: Vulkanologische Karte West- und Hocheifel, Landesvermessungsamt Rheinland-Pfalz, 1991.
- Büchel, G. and Mertes, H.: Die Eruptionen des Westeifeler Vulkanfeldes, *Z. Dtsch. Geol. Gesell.*, 133, 409–429, 1982.
- Canil, D. and Fedortchouk, Y.: Garnet dissolution and the emplacement of kimberlites, *Earth Planet. Sc. Lett.*, 167, 227–237, 1999.
- Chew, D. M., Petrus, J. A., and Kamber, B. S.: U–Pb LA–ICPMS dating using accessory mineral standards with variable common Pb, *Chem. Geol.*, 363, 185–199, 2014.
- de Capitani, C. and Brown, T. H.: The computation of chemical equilibrium in complex systems containing non-ideal solutions, *Geochim. Cosmochim. Ac.*, 51, 2639–2652, 1987.
- de Capitani, C. and Petrakakis, K.: The computation of equilibrium assemblage diagrams with Theriak/Domino software, *Amer. Miner.*, 95, 1006–1016, 2010.
- Dégi, J., Abart, R., Török, K., Bali, E., Wirth, R., and Rhede, D.: Symplectite formation during decompression induced garnet breakdown in lower crustal mafic granulite xenoliths: mechanisms and rates, *Contrib. Mineral. Petrol.*, 159, 293–314, 2010.
- Dèzes, P., Schmid, S., and Ziegler, P.: Evolution of the European Cenozoic Rift System: interaction of the Alpine and Pyrenean orogens with their foreland lithosphere, *Tectonophysics*, 389, 1–33, 2004.

- Ernst, W. G. and Liou, J. G.: High- and ultrahigh-pressure metamorphism: Past results and future prospects, *Amer. Miner.*, 93, 1771–1786, 2008.
- Faak, K., Chakraborty, S., and Coogan, L. A.: Mg in plagioclase: Experimental calibration of a new geothermometer and diffusion coefficients, *Geochim. Cosmochim. Ac.*, 123, 195–217, 2013.
- Faryad, S. W., Jedlicka, R., Hauzenberger, C., and Racek, M.: High-pressure crystallization vs. recrystallization origin of garnet pyroxenite-eclogite within subduction related lithologies, *Mineral. Petrol.*, 112, 603–616, 2018.
- Fekiacova, Z., Mertz, D. F., and Renne, P. R.: Geodynamic Setting of the Tertiary Hocheifel Volcanism (Germany), Part I: $^{40}\text{Ar}/^{39}\text{Ar}$ geochronology, in: *Mantle Plumes: A Multidisciplinary Approach*, edited by: Ritter, J. R. R. and Christensen, U. R., Springer, Berlin, Heidelberg, 185–206, 2007.
- Féménias, O., Coussaert, N., Bingen, B., Whitehouse, M., Mercier, J.-C. C., and Demaiffe, D.: A Permian underplating event in late- to post-orogenic tectonic setting. Evidence from the mafic-ultramafic layered xenoliths from Beaunit (French Massif Central), *Chem. Geol.*, 199, 293–315, 2003.
- Frost, B. R., Chamberlain, K. R., and Schumacher, J. C.: Sphene (titanite): phase relations and role as a geochronometer, *Chem. Geol.*, 172, 131–148, 2001.
- Green, D. H. and Ringwood, A. E.: The Genesis of basaltic magmas, *Contrib. Mineral. Petrol.*, 15, 103–190, 1967.
- Hajdas, I., Zolitschka, B., Ivy-Ochs, S. D., Beer, J., Bonani, G., Leroy, S. A. G., Negendank, J. W., Ramrath, M., and Suter, M.: AMS radiocarbon dating of annually laminated sediments from lake Holzmaar, Germany, *Quaternary Sci. Rev.*, 14, 137–143, 1995.
- Harley, S. L.: The origins of granulites: a metamorphic perspective, *Geol. Mag.*, 126, 215–247, 1989.
- Hartnady, M. I. H., Kirkland, C. L., Clark, C., Spaggiari, C. V., Smithies, R. H., Evans, N. J., and McDonald, B. J.: Titanite dates crystallization: Slow Pb diffusion during super-solidus re-equilibration, *J. Metamorph. Geol.*, 37, 823–838, 2019.
- Hayden, L. A., Watson, E. B., and Wark, D. A.: A thermobarometer for sphene (titanite), *Contrib. Mineral. Petrol.*, 155, 529–540, 2008.
- Hirschmann, M. M., Renne, P. R., and McBirney, A. R.: $^{40}\text{Ar}/^{39}\text{Ar}$ dating of the Skaergaard intrusion, *Earth Planet. Sc. Lett.*, 146, 645–658, 1997.
- Illies, J. H., Prodehl, C., Schmincke, H.-U., and Semmel, A.: The Quaternary uplift of the Rhenish shield in Germany, *Tectonophysics*, 61, 197–225, 1979.
- Keyser, M., Ritter, J. R. R., and Jordan, M.: 3D shear-wave velocity structure of the Eifel plume, Germany, *Earth Planet. Sc. Lett.*, 203, 59–82, 2002.
- Kramers, J. D. and Tolstikhin, I. N.: Two terrestrial lead isotope paradoxes, forward transport modelling, core formation and the history of the continental crust, *Chem. Geol.*, 139, 75–110, 1997.
- Lloyd, F. E. and Bailey, D. K.: Light element metasomatism of the continental mantle: The evidence and the consequences, *Phys. Chem. Earth*, 9, 389–416, 1975.
- Loock, G., Stosch, H.-G., and Seck, H. A.: Granulite facies lower crustal xenoliths from the Eifel, West Germany: petrological and geochemical aspects, *Contrib. Mineral. Petrol.*, 105, 24–41, 1990.
- Marzoli, A., Jourdan, F., Bussy, F., Chiaradia, M., and Costa, F.: Petrogenesis of tholeiitic basalts from the Central Atlantic magmatic province as revealed by mineral major and trace elements and Sr isotopes, *Lithos*, 188, 44–59, 2014.
- Mengel, K., Sachs, P. M., Stosch, H. G., Wörner, G., and Loock, G.: Crustal xenoliths from Cenozoic volcanic field of West Germany: Implications for structure and composition of the continental crust, *Tectonophysics*, 195, 271–289, 1991.
- Mertes, H.: Aufbau und Genese des Westeifeler Vulkanfeldes, *Bochumer Geologische und Geotechnische Arbeiten*, thesis, 9, 415 pp., 1983.
- Mertes, H. and Schmincke, H.-U.: Age Distribution of Volcanoes in the West-Eifel, *Neu. Jb. Geol. Paläont., Abh.*, 166, 260–293, 1983.
- Mertes, H. and Schmincke, H.-U.: Mafic potassic lavas of the Quaternary West Eifel volcanic field, *Contrib. Mineral. Petrol.*, 89, 330–345, 1985.
- Mertz, D. F., Loehnertz, W., Nomade, S., Pereira, A., Prelevic, D., and Renne, P.: Temporal-spatial evolution of low-SiO₂ volcanism in the Pleistocene West Eifel volcanic field (West Germany) and relationship to upwelling asthenosphere, *J. Geodyn.*, 88, 59–79, 2015.
- Meyer, W.: *Geologie der Eifel*, E. Schweizerbart'sche Verlagsbuchhandlung, Stuttgart, 1994.
- Nowell, D., Jones, M., and Pyle, D.: Episodic Quaternary volcanism in France and Germany, *J. Quat. Sci.*, 21, 645–675, 2006.
- Obata, M., Ohi, S., and Miyake, A.: Experimental synthesis of isochemical kelyphite – a preliminary report, *J. Mineral. Petrol. Sci.*, 109, 91–96, 2014.
- O'Brien, P. J. and Rötzler, J.: High-pressure granulites: formation, recovery of peak conditions and implications for tectonics, *J. Metamorph. Geol.*, 21, 3–20, 2003.
- Okrusch, M., Schroder, B., and Schnutgen, A.: Granulite-facies metabasite ejecta in the Laacher See area, Eifel, West Germany, *Lithos*, 12, 251–270, 1979.
- Paton, C., Hellstrom, J., Paul, B., Woodhead, J., and Hergt, J.: Iolite: Freeware for the visualisation and processing of mass spectrometric data, *J. Anal. Atomic Spect.*, 26, 2508–2518, 2011.
- Pearce, N., Perkins, W., Westgate, J., Gorton, M., Jackson, S., Neal, C., and Chenery, S.: A compilation of new and published major and trace element data for NIST SRM 610 and NIST SRM 612 glass reference materials, *Geostand. News.*, 21, 115–144, 1997.
- Petford, N. and Gallagher, K.: Partial melting of mafic (amphibolitic) lower crust by periodic influx of basaltic magma, *Earth Planet. Sc. Lett.*, 193, 483–499, 2001.
- Pozsgai, E., Józsa, S., Dunkl, I., Sebe, K., Thamó-Bozsó, E., Sajó, I., Dezső, J., and von Eynatten, H.: Provenance of the Upper Triassic siliciclastics of the Mecsek Mountains and Villány Hills (Pannonian Basin, Hungary): constraints to the Early Mesozoic paleogeography of the Tisza Megaunit, *Int. J. Earth. Sci.*, 106, 2005–2024, 2017.
- Prodehl, C.: Structure of the crust and upper mantle beneath the central European rift system, *Tectonophysics*, 80, 255–269, 1981.
- Prodehl, C., Mueller, S., Glahn, A., Gutscher, M., and Haak, V.: Lithospheric cross sections of the European Cenozoic rift system, *Tectonophysics*, 208, 113–138, 1992.
- Ritter, J. R. R., Jordan, M., Christensen, U. R., and Achauer, U.: A mantle plume below the Eifel volcanic fields, Germany, *Earth Planet. Sc. Lett.*, 186, 7–14, 2001.

- Rudnick, R. L. and Goldstein, S. L.: The Pb isotopic compositions of lower crustal xenoliths and the evolution of lower crustal Pb, *Earth Planet. Sc. Lett.*, 98, 192–207, 1990.
- Schmidberger, S. S. and Hegner, E.: Geochemistry and isotope systematics of calc-alkaline volcanic rocks from the Saar-Nahe basin (SW Germany) ± implications for Late-Variscan orogenic development, *Contrib. Mineral. Petrol.*, 135, 373–385, 1999.
- Schmincke, H. U.: The Quaternary Volcanic Fields of the East and West Eifel (Germany), in: *Mantle Plumes: A Multidisciplinary Approach*, edited by: Ritter, J. R. R. and Christensen, U. R., Springer, Berlin, Heidelberg, 241–322, 2007.
- Schnepf, E. and Hradetzky, H.: Combined paleointensity and $^{40}\text{Ar}/^{39}\text{Ar}$ age spectrum data from volcanic rocks of the West Eifel field (Germany): Evidence for an early Brunhes geomagnetic excursion, *J. Geophys. Res.*, 99, 9061–9076, 1994.
- Seiberlich, C. K. A., Ritter, J. R. R., and Wawerzinek, B.: Topography of the lithosphere–asthenosphere boundary below the Upper Rhine Graben Rift and the volcanic Eifel region, Central Europe, *Tectonophysics*, 603, 222–236, 2013.
- Shaw, C. S. J.: Dissolution of orthopyroxene in basanitic magma between 0.4 and 2 GPa: further implications for the origin of Si-rich alkaline glass inclusions in mantle xenoliths, *Contrib. Mineral. Petrol.*, 135, 114–132, 1999.
- Shaw, C. S. J.: Caught in the act – The first few hours of xenolith assimilation preserved in lavas of the Rockeskyllerkopf volcano, West Eifel, Germany, *Lithos*, 112, 511–523, 2009a.
- Shaw, C. S. J.: Textural development of amphibole during breakdown reactions in a synthetic peridotite, *Lithos*, 110, 215–228, 2009b.
- Shaw, C. S. J. and Edgar, A. D.: Post-entrapment mineral–melt reactions in spinel peridotite xenoliths from Inver, Donegal, Ireland, *Geol. Mag.*, 134, 771–779, 1997.
- Shaw, C. S. J. and Eyzaguirre, J.: Origin of megacrysts in the alkaline lavas of the West Eifel volcanic field, Germany, *Lithos*, 50, 75–95, 2000.
- Shaw, C. S. J. and Klügel, A.: The pressure and temperature conditions and timing of glass formation in mantle-derived xenoliths from Baarley, West Eifel, Germany: the case for amphibole breakdown, lava infiltration and mineral – melt reaction, *Mineral. Petrol.*, 74, 163–187, 2002.
- Shaw, C. S. J. and Woodland, A. B.: The role of magma mixing in the petrogenesis of mafic alkaline lavas, Rockeskyllerkopf Volcanic Complex, West Eifel, Germany, *Bull. Volcanol.*, 74, 359–376, 2012.
- Shaw, C. S. J., Eyzaguirre, J., Fryer, B. J., and Gagnon, J.: Regional Variations in the Mineralogy of Metasomatic Assemblages in Mantle Xenoliths from the West Eifel Volcanic Field, Germany, *J. Petrol.*, 46, 945–972, 2005.
- Shaw, C. S. J., Heidelberg, F., and Dingwell, D. B.: The origin of reaction textures in mantle peridotite xenoliths from Sal Island, Cape Verde: the case for “metasomatism” by the host lava, *Contrib. Mineral. Petrol.*, 151, 681–697, 2006.
- Shaw, C. S. J., Woodland, A. B., Hopp, J., and Trenholm, N.: Structure and evolution of the Rockeskyllerkopf Volcanic Complex, West Eifel Volcanic Field, Germany, *Bull. Volcanol.*, 72, 971–990, 2010.
- Shaw, C. S. J., Lebert, B. S., and Woodland, A. B.: Thermodynamic Modelling of Mantle–Melt Interaction Evidenced by Veined Wehrilite Xenoliths from the Rockeskyllerkopf Volcanic Complex, West Eifel Volcanic Field, Germany, *J. Petrol.*, 59, 59–86, 2018.
- Spandler, C., Hammerli, J., Sha, P., Hilbert-Wolf, H., Hu, Y., Roberts, E., and Schmitz, M.: MKED1: A new titanite standard for in situ analysis of Sm–Nd isotopes and U–Pb geochronology, *Chem. Geol.*, 425, 110–126, 2016.
- Stosch, H.-G.: Constitution and evolution of subcontinental upper mantle and lower crust in areas of young volcanism: Differences and similarities between the Eifel (F.R. Germany) and Tariat Depression (central Mongolia) as evidenced by peridotite and granulite xenoliths, *Fortsch. Mineral.*, 65, 49–86, 1987.
- Stosch, H. G., Lugmair, G. W., and Seck, H. A.: Geochemistry of granulite-facies lower crustal xenoliths: implications for the geological history of the lower continental crust below the Eifel, West Germany, *Geol. Soc. Lond. Spec. Pub.*, 24, 309–317, 1986.
- Stosch, H.-G., Schmucker, A., and Reys, C.: The nature and geological history of the deep crust under the Eifel, Germany, *Terra Nova*, 4, 53–62, 1992.
- Sun, C. and Liang, Y.: A REE-in-plagioclase–clinopyroxene thermometer for crustal rocks, *Contrib. Mineral. Petrol.*, 172, 24, <https://doi.org/10.1007/s00410-016-1326-9>, 2017.
- Sun, S.-S. and McDonough, W. F.: Chemical and isotopic systematics of oceanic basalts: implications for mantle composition and processes, *Geol. Soc. Lond. Spec. Pub.*, 42, 313–345, 1989.
- Tam, P. Y., Zhao, G., Sun, M., Li, S., Wu, M., and Yin, C.: Petrology and metamorphic P–T path of high-pressure mafic granulites from the Jiaobei massif in the Jiao-Liao-Ji Belt, North China Craton, *Lithos*, 155, 94–109, 2012.
- Timmerman, M. J., Heeremans, M., Kirstein, L. A., Larsen, B. T., Spencer-Dunworth, E.-A., and Sundvoll, B.: Linking changes in tectonic style with magmatism in northern Europe during the late Carboniferous to latest Permian, *Tectonophysics*, 473, 375–390, 2009.
- Upton, B. G. J., Stephenson, D., Smedley, P. M., Wallis, S. M., and Fitton, J. G.: Carboniferous and Permian magmatism in Scotland, *Geol. Soc. Lond. Spec. Pub.*, 223, 195–218, 2004.
- Van Orman, J. A., Grove, T. L., and Shimizu, N.: Rare earth element diffusion in diopside; influence of temperature, pressure and ionic radius, and an elastic model for diffusion in silicates, *Contrib. Mineral. Petrol.*, 141, 687–703, 2001.
- Vernon, R. H.: A practical guide to rock microstructure, Cambridge University Press, Cambridge, 2004.
- Witt-Eickchen, G., Kaminsky, W., Kramm, U., and Harte, B.: The nature of young vein metasomatism in the lithosphere of the West Eifel (Germany): Geochemical and Isotopic constraints from the composite mantle xenoliths from the Meerfelder Maar, *J. Petrol.*, 39, 155–185, 1998.
- Witt-Eickchen, G., Seck, H. A., Mezger, K., Eggins, S. M., and Altherr, R.: Lithospheric mantle evolution beneath the Eifel (Germany): Constraints from Sr–Nd–Pb isotopes and trace element abundances in spinel peridotite and pyroxenite xenoliths, *J. Petrol.*, 44, 1077–1095, 2003.
- Wohletz, K., Civetta, L., and Orsi, G.: Thermal evolution of the Phlegraean magmatic system, *J. Volcanol. Geotherm. Res.*, 91, 391–414, 1999.
- Wörner, G., Schmincke, H.-U., and Schreyer, W.: Crustal xenoliths from the Quaternary Wehr volcano (East Eifel), *Neu. Jb. Mineral. Abh.*, 144, 29–55, 1982.

Xirouchakis, D., Lindsley, D. H., and Andersen, D. J.: Assemblages with titanite (CaTiOSiO_4), Ca-Mg-Fe olivine and pyroxenes, Fe-Mg-Ti oxides, and quartz; Part I, Theory, *Amer. Miner.*, 86, 247–253, 2001a.

Xirouchakis, D., Lindsley, D. H., and Frost, B. R.: Assemblages with titanite (CaTiOSiO_4), Ca-Mg-Fe olivine and pyroxenes, Fe-Mg-Ti oxides, and quartz; Part II, Application, *Amer. Miner.*, 86, 254–264, 2001b.

Ziegler, P. A. and Dèzes, P.: Evolution of the lithosphere in the area of the Rhine Rift System, *Int. J. Earth. Sci.*, 94, 594–614, 2005.

Zolitschka, B., Negendank, J., and Lottermoser, B.: Sedimentological proof and dating of the early Holocene volcanic eruption of Ulmener Maar (Vulkaneifel, Germany), *Geol. Rund.*, 84, 213–219, 1995.